Assessing the Rosemount Icing Detector with In Situ Measurements

STEWART G. COBER, GEORGE A. ISAAC, AND ALEXEI V. KOROLEV

Cloud Physics Research Division, Meteorological Service of Canada, Downsview, Ontario, Canada

(Manuscript received 15 May 2000, in final form 8 August 2000)

ABSTRACT

In situ measurements of microphysics conditions, obtained during 38 research flights into winter storms, have been used to characterize the performance of a Rosemount Icing Detector (RID). Characteristics of the RID were determined under a wide range of cloud environments, which included icing conditions within mixed phase, freezing rain, and freezing drizzle environments. Cloud conditions observed included temperatures between 0° and −29°C and liquid water contents (LWCs) up to 0.7 g m^{-3}. The detection threshold for LWC was found to be 0.007 ± 0.010 g m^{-3} for the RID operated at an air speed of 97 ± 10 m s^{-1}, which agrees well with theoretical predictions. A signal level of 0 ± 2 mV s^{-1} accounted for 99.6% of the measurements in clear air and 98.5% of the measurements in glaciated clouds, when the data were averaged over 30-s intervals. No significant response to glaciated clouds was found during any of the research flights, implying that the instrument can be used to segregate glaciated and mixed phase clouds. There was no change in the RID response between liquid and mixed phase conditions, suggesting that ice crystals neither eroded ice accumulation nor accreted to the RID surface under the range of conditions experienced. During sustained icing conditions, a linear relationship between the RID signal and LWC was observed after the RID signal exceeded 400 mV above the clear-air signal level. The LWC derived from the RID was found to agree with LWC measurements from Nevzorov probes within ±50% for 92% of the data. The relationship between the RID signal and LWC was unchanged for freezing precipitation environments with drop median volume diameters >100 μm. The Ludlam limit was estimated for low LWC values and was found to agree well with theoretical calculations. The analysis provides considerable insight into the strengths and weaknesses of the instrument for operations in natural icing conditions.

1. Introduction

Following the systematic down-linking of temperature and wind data from commercial aircraft through the Aircraft Communications Addressing and Recording System (ACARS), there was a significant enhancement in the temporal and spatial accuracy of numerical forecast models (Fleming 1996). It was further estimated that down-linking of humidity data would increase the number of vapor profiles over the United States by a factor of 5 (Fleming 1996). The addition of icing detector measurements to ACARS has been discussed by Riley et al. (1999), and efforts are being undertaken to perform a trial experiment. In addition to the identification of potentially hazardous icing regions in real time, down-linked icing detector data would be extremely beneficial for the validation of aircraft icing numerical forecast algorithms. Currently, some validation techniques rely on pilot reports (Schwartz 1996; Kelsch and Wharton 1996), while others rely on data collected by research aircraft during field projects (Guan et al. 2001). The value of pilot reports is known to be limited by their nonquantitative assessments of the icing conditions and the bias toward the reporting of positive signals, while field project data tend to be biased toward meteorological conditions with stronger signals and are normally limited to a small number of flights. Assuming that quantitative assessments of icing environments could be down-linked, this would provide a unique opportunity for icing algorithm validation.

The U.S. Federal Aviation Administration and Transport Canada allow icing conditions detectors installed on commercial aircraft to be certified as either primary or secondary systems. A primary system will automatically activate anti-icing protection systems, while a secondary system will alert the pilot that icing conditions are being encountered. It is estimated that roughly half of the passenger-carrying commercial aircraft operated in North American air space are equipped with an icing detector. The majority of these aircraft are equipped with a Rosemount Icing Detector, which is manufactured by BF Goodrich Aerospace. Several research aircraft also include an RID among their instrumentation suites (Sand et al. 1984; Cober et al. 1995; Ashenden and Marwitz 1998; Brown 1982; Strapp et al. 1999; Hill 1991; Miller et al. 1998). While the majority of com-

Corresponding author address: Stewart Cober, Cloud Physics Research Division, Meteorological Service of Canada, 4905 Dufferin Street, Downsview, ON M3H 5T4, Canada.
E-mail: stewart.cober@ec.gc.ca

mercial aircraft do not currently have an ACARS capability, it is not unreasonable to assume that the potential for down-linking icing detector data will increase with the introduction of new aircraft and the continued development of communications systems such as ACARS. It is important, therefore to assess the capabilities of common icing detectors so that it is clear what research objectives (e.g., validation of icing forecast algorithms) might be achieved.

The RID is a magnetostrictive oscillation probe with a sensing cylinder 6.35 mm in diameter and 2.54 cm in length. Ice buildup on the sensing cylinder causes the frequency of oscillation to change, which can be related to the rate of ice accretion and hence the cloud liquid water content (LWC). When approximately 0.5 mm of ice has accumulated, a heater melts the ice, which is shed into the air stream. The heater cycle is approximately 5 s, and the cylinder normally requires an additional 5–10 s to cool down to a temperature where it can begin accreting ice again. A detailed description of the instrument is given in Baumgardner and Rodi (1989). The instrument is limited by the Ludlam limit (Ludlam 1951), which occurs when the LWC is sufficiently high that the surface temperature of the ice accumulation reaches 0°C. In such cases, the voltage signal may not be a reliable indicator of ice accumulation because the cloud droplets might not freeze to the sensing cylinder.

Characterizations of the RID capabilities in natural icing conditions are scarce. Baumgardner and Rodi (1989) assessed characteristics of an RID from a series of wind tunnel experiments and showed that for icing conditions below the Ludlam limit (Ludlam 1951) and for probes that were calibrated in a wind tunnel in terms of sensitivity to LWC, the RID was capable of estimating LWC within 20%. Brown (1982) concluded that the RID was a sensitive instrument at low LWC or cold temperature, but that its usefulness in cumulus clouds with high LWC was restricted by the Ludlam limit. Using data collected at temperatures colder than −40°C, where all hydrometeors were assumed to be ice crystals, Heymsfield and Miloshevich (1989) estimated the noise on their RID to be less than 3 mV s^{-1} for data evaluated at 1 s resolution. They also showed that the RID did not appear to respond to ice particles and had a detection threshold for LWC of approximately 0.002 g m^{-3} at temperatures colder than −20°C. Strapp et al. (1999) showed that ice accreted on an RID would undergo sublimation because of the adiabatic compression of the flow. This sublimation would cause a nonzero LWC threshold, which was estimated to be between 0.03–0.06 g m^{-3} for an aircraft traveling at 200 m s^{-1}. They also proposed that some of the noise on the RID might be related to small ice crystals that accreted along the stagnation line of the RID and rapidly sublimated. At a measurement speed of 200 m s^{-1}, they observed noise on the RID up to ±20 mV s^{-1} for data evaluated at 1-s resolution. Mazin et al. (2001) computed the theoretical heat and mass transfer for the RID and showed an LWC threshold of approximately 0.002–0.006 g m^{-3} for an aircraft flying at 100 m s^{-1}.

While RID measurements are often discussed when assessing cloud environments (Cooper et al. 1984; Politovich 1989; Cober et al. 1995; Strapp et al. 1999), there has been no extensive summary of how well the instrument performed over a wide range of natural icing conditions. In this paper, the capabilities of an RID are assessed based on data obtained during 38 research flights in winter storm conditions. The dataset included numerous freezing drizzle, freezing rain, and mixed phase environments over a wide range of LWC and temperature conditions.

2. Field projects

The Meteorological Service of Canada (MSC) RID was originally mounted on the National Research Council (NRC) Convair-580 during the Second Canadian Atlantic Storms Program (CASP II), which was conducted during the winter of 1992 (Stewart 1991). Cober et al. (1995) stated that inconsistent LWC results were obtained with the RID during CASP II and that consequently it was not used to estimate LWC during icing encounters. The RID was mounted on the top of the fuselage behind the pilot's window, and it is believed that this region was a partially shadowed region for cloud drops. This is the likely explanation for the poor RID correlation with LWC during CASP II. The RID was tested in the NRC high-speed wind tunnel in 1994 and 1997 in a similar manner to that described by Baumgardner and Rodi (1989). In both cases it was found to be working correctly (see section 4d).

Subsequent to CASP II, the RID location was changed to the starboard wing. It was mounted on the underside of the wing, 1.41 m from the leading edge and 5.5 m from the wing tip. The sensing cylinder of the RID was 5–7 cm from the wing surface. A discussion of the revised instrument mounting location will be presented in section 4e. The RID was flown during the First and Third Canadian Freezing Drizzle Experiments (CFDE I and III, respectively), which were conducted during the winters of 1995 and 1997/98, respectively. These projects were designed to measure microphysical parameters in regions of winter storms where freezing drizzle conditions were observed or expected to develop (Isaac et al. 1999). During CFDE I and III, there were 38 research flights conducted representing approximately 21 000 km of flight in clouds at temperatures colder than 0°C. The data include temperatures between 0° and −29°C, LWC up to 0.7 g m^{-3}, and pressure between 42 and 101 kPa. This dataset is well suited for assessing the capabilities of an RID in a wide variety of icing environments.

3. Instrumentation

The NRC Convair-580 was fully instrumented for microphysical measurements, as described in Isaac et al. (1999). The majority of important parameters (e.g., temperature, pressure, LWC, droplet concentration) were measured with two or three instruments to allow for redundancy and intercomparisons and to minimize the effects of a malfunctioning instrument. Instruments were mounted on three under-wing pylons, including a dedicated pylon for the LWC probes and two pylons for holding Particle Measuring System (PMS)-type probes. Flow effects for the LWC pylon were measured following the technique of Drummond and MacPherson (1985), and the LWC corrections for all the LWC probes were determined to be between 3% and 5%. Flow corrections for the PMS pods (King 1986) were not incorporated in the analysis because the associated measurement biases were estimated to be significantly less than the probe measurement accuracies.

Temperature was measured with two Rosemount temperature probes and a reverse flow temperature probe, which normally agreed within $\pm 1^{\circ}$C. Dewpoint was measured within $\pm 2^{\circ}$C with a Cambridge dewpoint hygrometer. LWC was measured with two PMS King probes (King et al. 1978) and a Nevzorov LWC probe (Korolev et al. 1998b). These instruments normally agreed within $\pm 15\%$ for LWC > 0.1 g m^{-3} and within 0.02 g m^{-3} for LWC < 0.1 g m^{-3} (Cober et al. 1999). Total water content (TWC), consisting of liquid and ice water content, was measured with a Nevzorov TWC probe (Korolev et al. 1998b). Two PMS forward scattering spectrometer probes (FSSPs) measured droplets between 3–45 and 5–95 μm, respectively, in 15 distinct size bins. Hydrometeor spectra were measured with 3 PMS 2D probes, including 2D–C mono 25–800 μm, 2D–C grey 25–1600 μm, and 2D–P mono 200–6400 μm. A Rosemount model 871FA221B icing detector was mounted under the starboard wing just behind the pylon that held the LWC probes. Figure 1 shows the location of the LWC pylon and RID for the NRC Convair-580 aircraft.

The King and Nevzorov probes were calibrated in several wind tunnel experiments conducted before and after the field projects (King et al. 1985; Cober et al. 1995; Korolev et al. 1998b; Strapp et al. 2000). During post-project analysis, the data for each instrument were carefully quality controlled and the zero signals were identified and subtracted from the LWC signals. The FSSPs were calibrated frequently with glass beads throughout each project, and the data were processed following Cober et al. (1995). The measured droplet concentrations agreed with each other within $\pm 30\%$. The scatter is higher than the expected $\pm 16\%$ demonstrated by Baumgardner (1983). Occasional icing of the probe tips as well as partial fogging of the optics during frequent aircraft ascents and descents are believed to explain the scatter in the FSSP data. Measurements in the first four channels of the PMS 2D probes were discarded because of depth-of-field uncertainties and significant sizing and concentration errors, which occur in these channels (Korolev et al. 1998a). In addition, identification of 2D particle shape is subject to considerable error for particles less than 10 pixels in diameter (Cober et al. 2000), and no attempts were made to identify particle images that were smaller than 5 pixels in diameter.

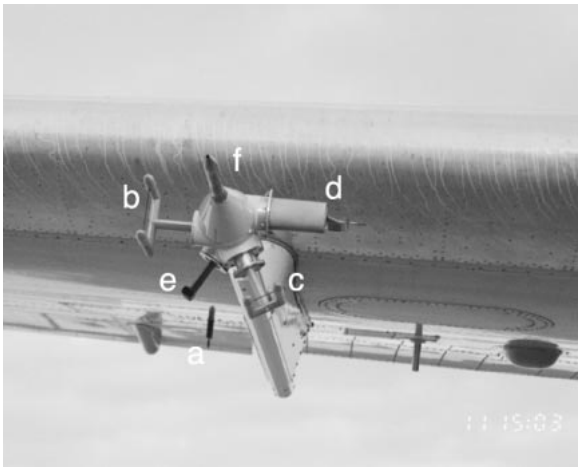

FIG. 1. Photograph of the mounting location of the (a) MSC RID under the starboard wing of the NRC Convair-580. The LWC pylon, which extends ahead of the wing leading edge, includes (b,c) two King probes, (d) Nevzorov LWC and TWC probes, (e) Rosemount temperature probe, and (f) Pitot tube.

Collectively, the FSSP and 2D probes covered the hydrometeor spectra from 3 to 6400 μm, thereby including cloud droplets, drizzle, raindrops, and ice crystals. Regions where no probe overlap occurred (i.e., between 95 and 125 μm or 800 and 1000 μm) were interpolated. Cloud phase was assessed as being liquid, mixed, or glaciated following techniques discussed in Cober et al. (2000). A brief outline of these techniques will be discussed in section 4f. For each droplet spectra that was derived from the FSSP and 2D measurements, the bulk collision efficiency with the RID was determined using the collision efficiency calculations of Finstad and Lozowski (1988). This is considered more accurate than using the collision efficiency of the spectra median volume diameter (MVD).

4. Analysis and discussion

a. Data averaging

The microphysical data were averaged at 30-s resolution. A 30-s averaging interval was selected to ensue that the measurements made with the 2D instruments contained sufficient particle counts for statistical significance. The 2D measurements were required because there was often significant LWC in drops > 100 μm. The periods of unusable data following each de-icing

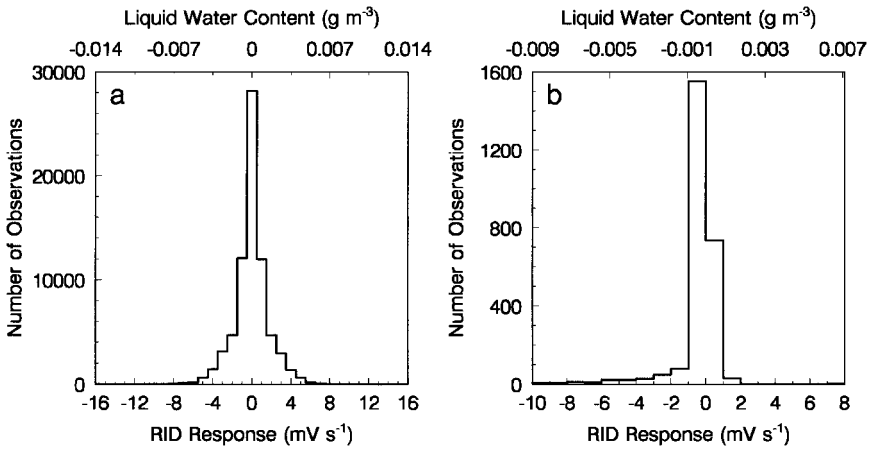

FIG. 2. Average response of the MSC RID in clear-air conditions for (a) 1-s data (72 851 observations) and (b) 30-s averaged data (2708 observations). The equivalent LWC is shown for comparison.

cycle were excluded from the RID averages so that the RID measurements represent the average response in millivolts per second for the good data in each 30-s period. In the event that the LWC, FSSP, or 2D probes were not working correctly, the data points were removed from the dataset. Examples of probe failures included fogging of the FSSP optics, which caused a falloff in the particle sizing; icing of the probe tips for the 2D probes, which usually caused streaker images to predominate; and poor identification of the zero level of the LWC probes. Data from each instrument were carefully examined in order to remove bad data from the dataset. In total, there were 6900 in-cloud data points collected during the CFDE I and III flights. This data included 3500 complete RID icing cycles.

b. RID noise level

Heymsfield and Miloshevich (1989) estimated the noise level on an RID by examining the 1-s signal in clouds with temperatures colder than −40°C (where it was assumed that there was no LWC). They found that the noise level was always ≤ 3 mV s^{-1} and that the majority of data had a noise level of ≤ 1 mV s^{-1}. This was consistent with the 1-mV resolution of the RID signal. It is possible that some of the noise observed by Heymsfield and Miloshevich (1989) was caused by the accretion of ice crystals. Strapp et al. (1999) suggested that small crystals colliding along the stagnation line could accrete and sublimate and that this might account for part of the signal observed on their RID. The noise on the MSC RID was estimated by examining the 1-s RID signal in regions of clear air. Clear air was identified when the Nevzorov TWC = 0.000 g m^{-3} for 3 consecutive seconds. Figure 2a shows a histogram of the 1-s changes in RID voltage for the clear air regions. RID responses that exceeded ± 5 mV s^{-1} and ± 2 mV s^{-1} accounted for 2% and 20% of the observations, respectively. The results show greater scatter than those of Heymsfield and Miloshevich (1989). Differences in the number of points used and in methodologies for extracting RID noise explain the differences between the results from these investigations. The RID response shown in Fig. 2a was reduced when the data were averaged at 30 s. Clear-air regions for the 30-s data were identified when the Nevzorov TWC and LWC <0.005 g m^{-3}, FSSP concentrations <0.1 cm^{-3}, and no particle images were identified on the 2D probes. Figure 2b shows a histogram of 2708 RID measurements made in clear air. In Fig. 2b, RID response refers to the voltage change per second averaged for each 30-s interval. The tail of negative values is caused by sublimation of ice off the RID following exit from a cloud. Neglecting the negative values that are caused by sublimation, a threshold of ± 2 mV s^{-1} accounts for 99.6% of the RID responses in clear air. This corresponds to an LWC of approximately 0.002 g m^{-3} (section 4d). The few data points with RID responses >2 mV s^{-1} were all associated with misidentification of clear-air regions, which was confirmed by examining the 1-s, FSSP and Nevzorov data. There was no evidence of a small drift in the RID voltage with temperature as discussed by Heymsfield and Miloshevich (1989).

c. Reset threshold

Following a de-icing cycle, the sensing cylinder of the RID must cool down to a temperature less than 0°C before it will start to accrete ice again. This reset period has been discussed by Baumgardner and Rodi (1989) and Mazin et al. (2001). Baumgardner and Rodi (1989) found that between 13 and 24 s were required before their RID signal regained a linear response to LWC, while Mazin et al. (2001) commented that 10%–90% of the measurement cycle could be incorporated into the reset periods. In order to quantify the reset cycle, periods

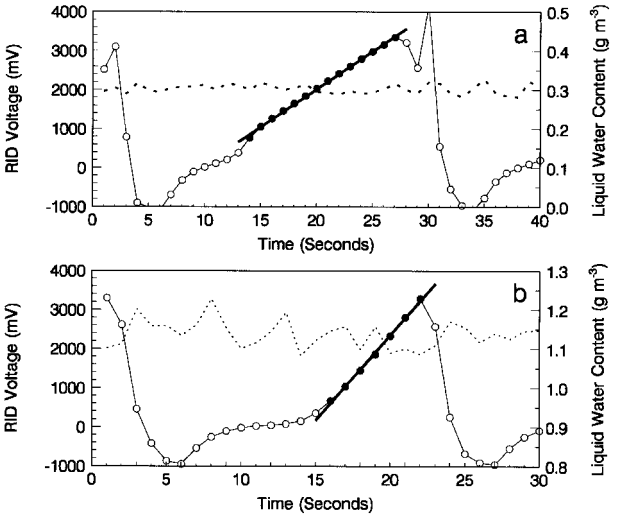

FIG. 3. Time history of the RID signal during wind tunnel experiments where the LWC was held constant. The 1-s LWC is shown by the dashed curves, while the 1-s RID signal is shown with open circles. The solid circles represent the 1-s RID data that were used to determine the best linear fit. The best fit is shown as a thick solid line. The temperatures were (a) −8.4°C and (b) −2.8°C. The LWC in (b) significantly exceeded the Ludlam limit.

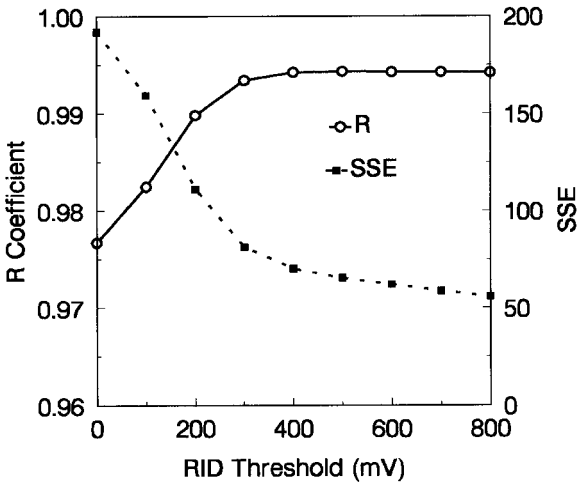

FIG. 4. Variation of the average SSEs and *R* with threshold RID voltage. These data represent averages of 1440 observations from CFDE III. Each observation represented an RID icing cycle during which the LWC was relatively constant.

of relatively constant LWC were identified from the wind tunnel and aircraft data. A constant LWC was assessed if the standard deviation for the 1-s LWC data over the period of the RID icing cycle was less than 20% of the mean LWC. For each RID icing cycle within a constant LWC period, the RID signal values at 1-s resolution were fit linearly from the time when the RID signal rose above a specified threshold value to the last RID value before the de-icing cycle started. For each fit, a correlation coefficient *R* was determined. This is illustrated in Fig. 3, which shows two RID icing cycles at LWC values of 0.30 ± 0.01 and 1.12 ± 0.03 g m^{-3}, respectively, where the error represents the standard deviation of the 1-s LWC values over the respective icing cycles. The LWC values shown in Fig. 3 were measured with a King probe. The RID threshold voltage was 400 mV so that RID >400 mV were used for the linear fits. The *R* coefficients were 0.99 for both fits. It is clear that the RID–LWC correlations in Fig. 3 are linear above the threshold value. It should be noted that in clear air, the RID voltage signal is normally between 1000 and 2000 mV. This offset was subtracted from the data shown in Fig. 3 so that a value of 0 mV in Fig. 3 represents the RID signal that would be expected in clear air.

The data for each RID icing cycle were fitted for several thresholds between 0 and 1000 mV. Figure 4 shows the variation of the average sum of squared errors (SSEs) and *R* coefficients for 1400 RID icing cycles as a function of threshold. The optimum threshold is a balance between the minimum sum of squared errors, the maximum *R* coefficient, and proximity of the threshold value to 0 mV. A threshold of 400 mV incorporates a relatively constant sum of squared errors and *R* coefficients, and this value was selected as the optimum threshold. For 2320 RID icing cycles with constant LWC, assuming an RID threshold of 400 mV, the *R* coefficient exceeded 0.97 and 0.99 for 99% and 88% of the data, respectively.

There were 2423 RID icing cycles observed during the wind tunnel experiments, CFDE I and CFDE III, where the LWC remained approximately constant through the subsequent de-icing period. For these cases, the average time required from the start of a de-icing cycle to the time when the RID reached the threshold of 400 mV was 15 ± 4 s, where the error represents the standard deviation. This is consistent with the results of Baumgardner and Rodi (1989). The length of the de-icing cycle was slightly dependent on LWC and strongly dependent on temperature, decreasing with increasing LWC and decreasing temperature. Ignoring the dependence on LWC, the de-icing cycle ranged from 13 ± 4 s for temperatures <−6°C, to 16 ± 3 s for temperatures between −3° and −6°C, to 19 ± 3 s for temperatures between −1° and −3°C. These trends are consistent with colder air temperatures or higher LWC, causing an increase in the cooling rate for the RID following a de-icing cycle. Since the majority of the in situ and tunnel measurements were made at air speeds (V_e) between 86 and 100 m s^{-1}, the effects of V_e on the length of the de-icing cycle were not assessed. Presumably, a higher V_e would also decrease the duration of the de-icing cycle. Heymsfield and Miloshevich (1989) found that an average of 90 sec was required before the data were considered reliable following a de-icing cycle. These long de-icing periods were probably caused by the temperatures at which they made their observations. This is demonstrated in Fig. 5, which shows observations from a flight on 17 February 1998 where the Convair-

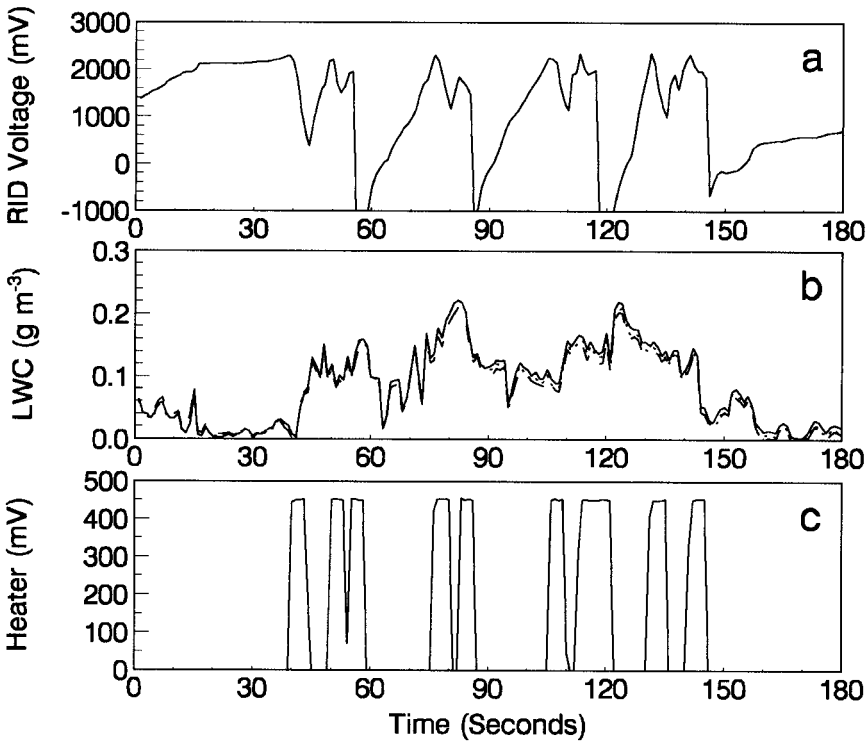

FIG. 5. Time history of (a) RID voltage, (b) LWC measured with three probes, and (c) RID de-icing heater voltage for an 180-s period from a flight on 17 Feb 1998. The measurements were made at temperatures between −18° and −20°C.

580 was flying at a relatively constant altitude at −18 to −20°C. Each de-icing cycle required 2–3 de-icing heater cycles (Fig. 5c) to fully shed the accumulated ice. This would be caused if the de-icing heaters were not able to provide enough heat to melt the ice at the ice–RID surface. The data collected by Heymsfield and Miloshevich (1989) were obtained at temperatures colder than −20°C. Hence, the data in Fig. 5 are consistent with explaining the long de-icing cycle durations found by Heymsfield and Miloshevich (1989). For algorithms that compute icing intensity or LWC based on the frequency of the heater de-icing cycles, these calculations would be in error in regions with temperatures < -18°C.

d. Correlation with LWC

Baumgardner and Rodi (1989) suggested that calibration of an RID in a wind tunnel should allow LWC to be inferred within ±20% from an RID signal. Assuming that mass transfer by sublimation, as discussed in Mazin et al. (2001), is a second-order effect and can be ignored (i.e., <0.01 g m^{-3}), the slope k is related to LWC and the RID response as

$$\frac{dV}{dt} = kEAV_e\text{LWC}, \tag{1}$$

where A is the area of sweep out for the RID, E the collision–collection efficiency of supercooled cloud droplets, and dV/dt the rate of change of voltage with time for the RID. Eq. (1) illustrates that the slope k will be influenced by the V_e and E used in the calibration. Figure 6 shows the relationship between LWC sweep out in grams per second ($=EAV_e$LWC) and RID voltage change in millivolts per second for a) in situ measurements from CFDE I and III and b) wind tunnel measurements from experiments conducted in 1994 and 1997. The in situ data were carefully screened and included only cases where the aircraft was flying at a true air speed (V_e) = 97 ± 10 m s^{-1} with minimum changes in altitude and heading, negligible ice water contents, and temperature < -5°C. The tunnel conditions included liquid phase cases with V_e = 86 ± 2 m s^{-1}, temperature < -6°C, and droplet MVD = 19 ± 3 μm. In situ LWC measurements were made with Nevzorov LWC and TWC probes, while a King probe was used for the wind tunnel measurements. The temperatures were selected to avoid Ludlam limit effects (section 4h). The data appear to be linear, and the best fit is shown for each case. There is a significant difference between the best fits with the slope changing from 81.0 V g^{-1} for the in situ data to 61.6 V g^{-1} for the wind tunnel measurements. Differences in V_e and E between the two datasets are already incorporated into the calculations and hence do not explain the 24% difference in the k values. The difference is possibly caused by compression and acceleration of the airflow for the flow around

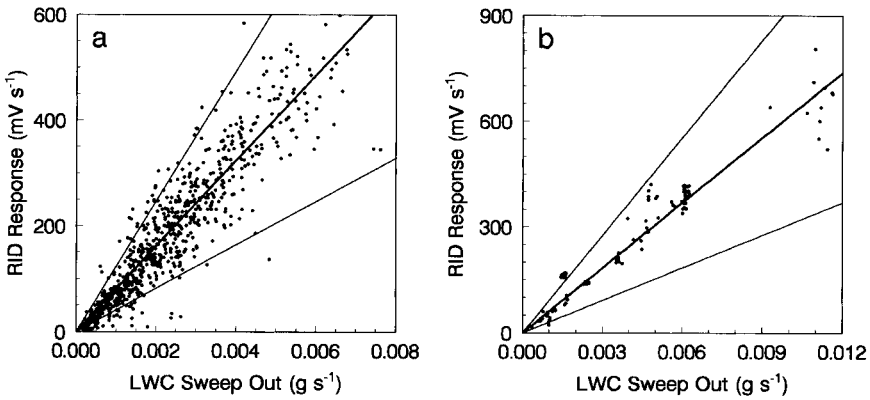

FIG. 6. Scatterplots of LWC sweep out vs average RID response for 30-s averaged data for (a) in situ observations (772 data points) and (b) wind tunnel observations (131 data points). The best-fit and ±50% curves are also shown.

the wings of the Convair-580. Both effects will enhance the effective mass sweep out rate (i.e., LWC) by the RID. The RID is approximately 5–7 cm from the wing surface, and the wing at its maximum thickness is approximately 25 cm thick. As discussed in section 3, the LWC probes were mounted ahead of the wing to avoid such an enhancement. Hence, it is not unreasonable to estimate that some of the LWC enhancement in the RID response for in situ measurements compared to tunnel measurements is caused by compression and acceleration of the airflow at the location of the RID. For the wind tunnel measurements, the RID and a King probe were mounted in locations where the LWC was constant within 5% (King et al. 1985). Hence, measurement errors for the tunnel LWC do not account for the differences in slopes observed. For both the in situ and wind tunnel measurements, the measured droplet spectra was used to infer the collision efficiencies for each droplet size with the RID. Hence, differences in MVD, V_e, and E between the datasets do not account for the observed differences in k.

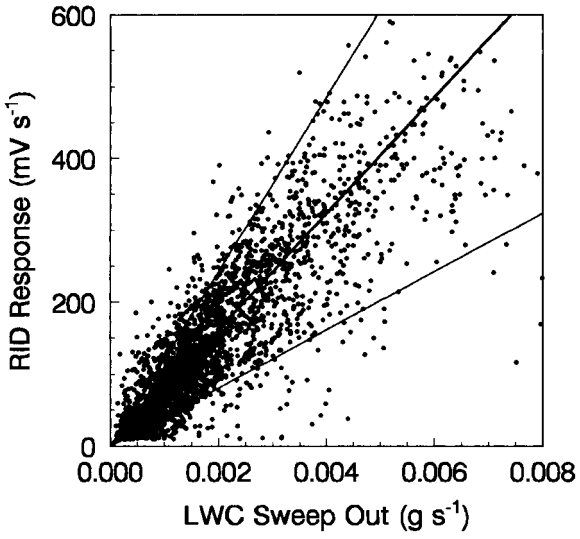

FIG. 7. Scatterplot of LWC sweep out vs average RID response for 5-s averaged data (3470 points). The best-fit and ±50% curves from Fig. 6a are also shown.

Figure 6 also shows ±50% curves. The in situ data show more scatter than the tunnel data, which is expected given the greater changes in environmental conditions encountered during icing cycles, particularly in terms of LWC and V_e. For the in situ and tunnel measurements where the LWC >0.1 g m^{-3}, 92% and 88% of the data, respectively, fall within the ±50% curves while 60% and 80%, respectively, fall within ±20% of the best fit curves. The tunnel results are relatively consistent with the ±20% LWC accuracy estimate of Baumgardner and Rodi (1989); however, the in situ results are not. Changes in the droplet distribution MVD, cloud temperature, and aircraft V_e will cause greater scatter for in situ data in comparison to the wind tunnel data. This is because LWC, temperature, and MVD are normally held at constant values in wind tunnel investigations. The use of a fixed averaging interval could add scatter to the in situ data. For example, the measurements of temperature and LWC for a 30-s period will normally represent an average of the 1-s data throughout the interval. Conversely, after removing data associated with the de-icing cycle, the RID signal may only include, for example, 10 to 15 s of good data during the 30-s period, and this data will probably be biased toward the start or end of the interval. If the LWC signal is variable over a 30-s period, this difference in the averaging interval will add scatter to the LWC–RID correlation. The in situ data were averaged at 5- to 120-s scales to assess whether the averaging interval affected the scatter or the slope of the curve shown in Fig. 6a. Figure 7 shows the RID response for the 5-s averages. The best-fit slope and ±50% curves from Fig. 6a are also shown for comparison. The data are very similar to those in Fig. 6a, with 90% of the data with LWC >0.1 g m^{-3} falling within the ±50% curves. Similar

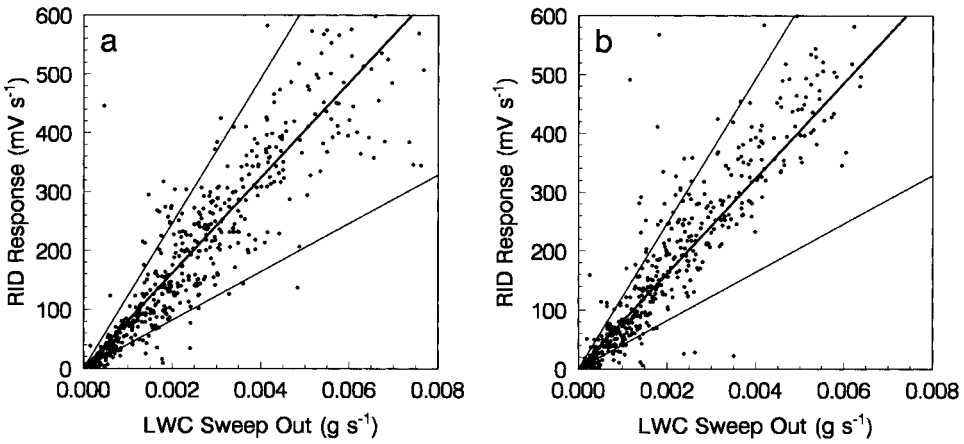

FIG. 8. Scatterplots of LWC sweep out vs average RID response for (a) altitude changes <30 m during each 30-s period (516 observations) and (b) altitude changes of >100 m during each 30-s period (475 observations). The best-fit and ±50% curves from Fig. 6a are also shown.

results were observed for averages at 60 and 120 s. It is concluded that the choice of averaging interval did not affect the slope k and did not add significant scatter to the data shown in Fig. 6a.

e. Mounting location

It is common practice to mount an RID on the fuselage of an aircraft in a location where the flow is expected to be streamlined along the fuselage and no shadowing effects are expected. In order to assess whether there was a location-dependent effect on the RID data, the in situ data were examined for trends for changes in aircraft flight characteristics. For example, Fig. 8 shows a scatterplot of RID versus LWC sweep out for flight at a) constant altitude and b) during ascent or descent that exceeded 200 m min^{-1}. The best-fit and ±50% curves from Fig. 6 are also shown for comparison. The R^2 coefficients with respect to the best-fit curve of Fig. 6a were 0.83 and 0.88 for the data in Figs. 8a and 8b, respectively. There is no significant difference between these data, indicating that ascent or descent did not affect the RID response characteristics. A similar result was found for changes in aircraft heading (i.e., banking). To investigate whether the mounting location might preferentially affect different drop sizes, the RID response was examined for different MVD values. Figure 9 shows the RID response for a) MVD between 10 and 15 μm and b) MVD between 20 and 30 μm. Using the formulations of Finstad and Lozowski (1988), the collision efficiencies for these MVD ranges are 0.81 ± 0.03 and 0.92 ± 0.01, respectively, assuming V_e = 97 m s^{-1}, temperature = −5°C, and the RID cylinder diameter of 6.35 mm. The best-fit and ±50% curves from Fig. 6a are also shown for comparison. The data in Figs. 9a and 9b have R^2 values of 0.92 and 0.65, respectively, with respect to the best fit from Fig. 6a. Although the data in Fig. 9b show a greater scatter, the R^2 values for data with MVD between 15–20 μm and 30–100 μm were 0.75 and 0.80, respectively, and the

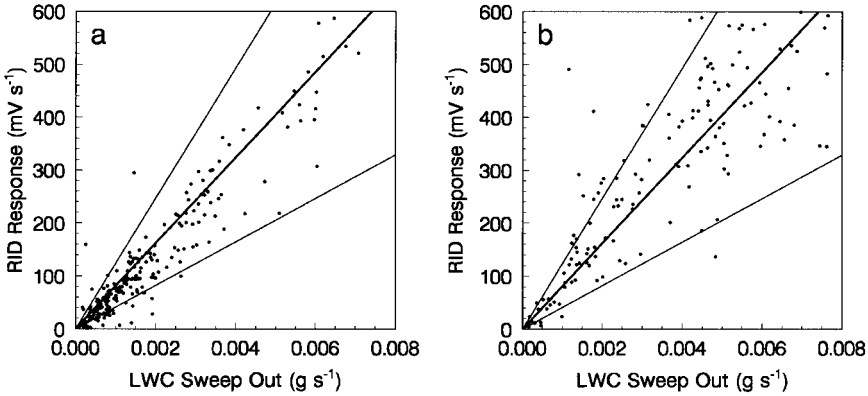

FIG. 9. Scatterplots of LWC sweep out vs average RID response for (a) MVD between 10 and 15 μm (220 observations) and (b) MVD between 20 and 30 μm (146 observations). The best-fit and ±50% curves from Fig. 6a are also shown.

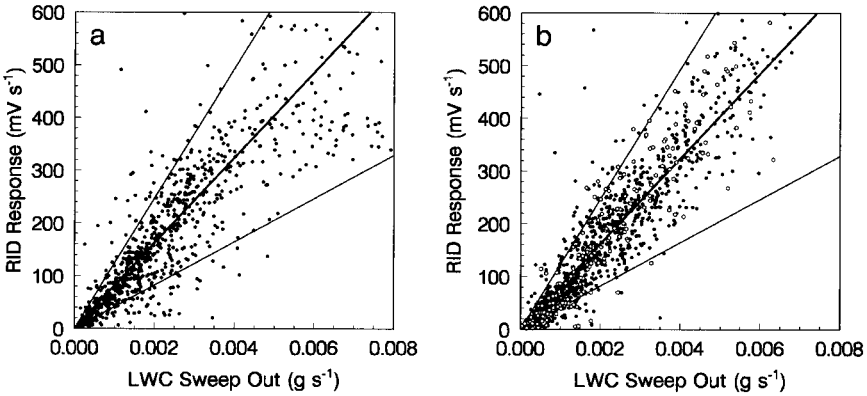

FIG. 10. Scatterplots of LWC sweep out vs average RID response for (a) liquid phase clouds with minimal ice crystals (855 observations) and (b) mixed phase clouds with significant ice crystals (1148 observations). Temperatures ranged from −5° to −22°C. Open circles represent cases with ice crystal concentrations >5 L^{-1} for particles >125 μm and temperatures <−5°C.

data are highly correlated with the best-fit curve from Fig. 6a. It is concluded that the mounting location has no significant shadowing effects for different sized droplets and that any such effect cannot be segregated from the scatter in the data.

f. Effects of cloud phase

To assess the effects of ice crystals on the RID response, the data were segregated into liquid and mixed phase conditions. Liquid phase conditions were assessed when the LWC and TWC measurements agreed within ±15% and when there was agreement between the FSSP-measured LWC and concentration measurements within the errors expected for such a comparison. A liquid phase classification also required that >90% of the classified 2D images with diameters ≥125 μm could be interpreted as circular images. In such cases, these circular images were interpreted as drops. Using data collected in clouds where the temperatures were >1°C, and hence all 2D images (less spurious artifacts) could be interpreted as drops, Cober et al. (2000) showed that geometric ratios involving particle area, perimeter, diameter, and symmetry could be used to identify >90% of the 2D images as circles. Some of the cases classified as liquid phase may have contained ice crystals; however, the concentrations were low and the ice water content was negligible. In cases with significant water content in drizzle or rain drop sizes, the LWC probes would underestimate the LWC because of their detection falloff for larger drop sizes (Biter et al. 1987; Strapp et al. 2000). In such cases the LWC:TWC ratio may have differed by more than 15%. In cases with no particles >125 μm, the 2D probes were not used in the phase assessment.

Mixed phase cases were identified from the cases that remained after the liquid and glaciated cases were identified. Mixed phase cases required that the LWC:TWC ratios were between 1:4 and 1:1, that there were characteristic ice and LWC responses on the FSSP probes (Gardiner and Hallett 1985; Cober et al. 2000; Cober et al. 1995), and that there were ice crystals (i.e., noncircular images) observed with the 2D probes. The data were further screened by eliminating all cases with temperature >−5°C in order to avoid Ludlam limit–related temperature limitations on the RID (see section 4h). Figure 10 shows the RID response for liquid and mixed phase conditions observed during CFDE I and CFDE III. The best-fit curve and ±50% curves from Fig. 6a are also shown for comparison. The R^2 coefficients for the liquid and mixed phase data with respect to the best fit curve in Fig. 6a are 0.81 and 0.88, respectively. The mixed phase data show a slightly higher response rate compared to the liquid phase cases; however, the trend is within the scatter of the data. Therefore, the presence of ice crystals in a mixed phase environment does not appear to cause a significant difference in RID response rate for the Convair-580 RID operated at 100 m s^{-1}. This is consistent with the observations of Heymsfield and Miloshevich (1989). Bain and Gayet (1982) observed that the presence of ice crystals >200 μm in concentrations >5 L^{-1} at temperatures <−8°C reduced the icing accumulation rate on an icing cylinder by approximately 50%. Cases in Fig. 10b with ice crystal concentrations >5 L^{-1}, temperature <−5°C, and sizes ≥125 μm accounted for 16% of the data points and are shown as open circles. There was no difference in the RID–LWC correlation for these data, which is contrary to the observations of Bain and Gayet (1982). Their measurements were taken in cumuliform clouds, and it is possible that the majority of the ice particles they observed were graupel. Sand et al. (1984) commented that graupel showers had effectively cleaned ice off of the leading edge of their aircraft. During CFDE I and III, graupel particles were rarely observed, and the largest crystals tended to be dendritic or irregular in shape. Graupel particles would contain substantially more mass

and momentum, which presumably would make them more effective in eroding ice.

Heymsfield and Miloshevich (1989) used glaciated cloud conditions at temperatures colder than −40°C to determine the noise level on their RID. They assumed that the instrument did not respond to ice particles, which is consistent with the observations discussed above. However, Strapp et al. (1999) indicated that some noise might be related to small ice crystals that accreted along the stagnation line of the cylinder and sublimated. In order to investigate these ideas, the glaciated phase regions were identified from the CFDE I and III data. Glaciated phase cases were identified by collectively assessing the characteristic signals on each probe (see Cober et al. 2000). Median volume diameters >20 μm on the FSSPs and FSSP particle concentrations <15 cm^{-3} are normally characteristic of a glaciated cloud (Cober et al. 2000; Cober et al. 1985; Gardiner and Hallett 1985). Similarly, King and Nevzorov LWC signals that were less than 15%–20% of the TWC signal are also characteristic of glaciated cloud conditions (Korolev et al. 1998b; Cober et al. 2000). Finally, the predominance of noncircular images in the 2D data is consistent with glaciated cloud. Cober et al. (2000) has shown that glaciated cloud conditions will normally have >60% of the particle images classified as noncircular. When assessed collectively, these techniques provide an accurate identification of glaciated phase conditions. Glaciated conditions were identified for temperature <−3°C, FSSP concentrations <10 cm^{-3}, MVD >20 μm, percentage of noncircular 2D images >70%, and ratio of LWC:TWC <0.15. In addition, the 1-s data were screened to ensure that selected regions of glaciated cloud did not have small pockets of embedded LWC. Using this restrictive screening, there were 203 data points that were identified as being entirely glaciated of which 200 had an RID signal ≤2 mV s^{-1}. The remaining three data points had an RID <3 mV s^{-1}. Therefore, 98.5% of the entirely glaciated cases identified from CFDE I and III had an RID signal that could not be distinguished from the mean zero signal in clear air. This supports the observations of Heymsfield and Miloshevich (1989) and the results in Fig. 10.

g. Response to freezing precipitation

To investigate the response of the RID under freezing precipitation conditions, the RID signal was examined for cases with MVD >100 μm. Figure 11 shows the RID response for liquid and mixed phase cases with temperature <−2.5°C and MVD ≥100 μm. The largest MVD value in Fig. 11 is approximately 1000 μm. The Nevzorov total water content measurement was used in the analysis because it is a more accurate measurement of LWC when the cloud drops exceed 100 μm in diameter, considering the fall off of the LWC probes for large drops (Biter et al. 1987; Strapp et al. 2000). The best fit has a slope of 76.5 V g^{-1}, which is within 6% of the slope for the data in Fig. 6a. The data in Fig. 11 had a V_e of 90 ± 10 m s^{-1} and collision efficiency (Finstad and Lozowski 1988) of 0.98 versus a V_e of 97 ± 10 m s^{-1} and collision efficiency of 0.81–0.92 for MVD between 12–30 μm, respectively, for the bulk of the data in Fig. 6a. The slope k includes the dependencies on V_e and E. This analysis suggests that there is no significant difference in the response of the RID to large drops and that any effect of MVD on the RID–LWC relationship is within the scatter of the data. It also suggests that large supercooled drops do not lose a significant portion of their mass by splashing or shedding when they collide with the RID.

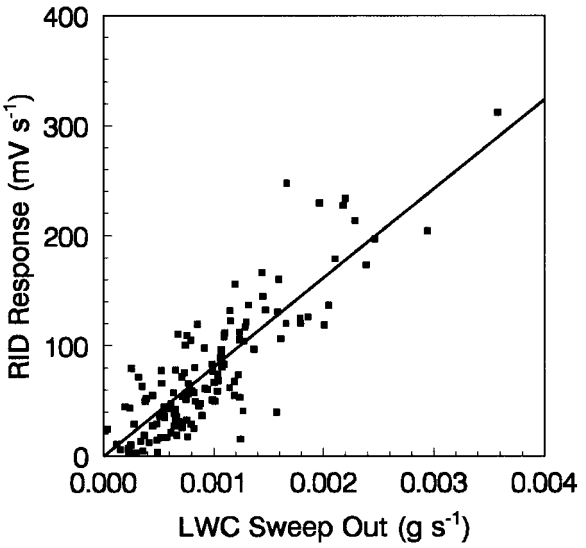

FIG. 11. Scatterplot of LWC sweep out vs average RID response for cloud intervals with MVD >100 μm (130 points). The data include liquid and mixed phase cases with temperature <−2.5°C and LWC less than the Ludlam limit. The best-fit curve from Fig. 6a is also shown.

h. Effect of temperature

The Ludlam limit occurs when the LWC is sufficiently high enough that the surface temperature of the ice accumulation can reach 0°C (Ludlam 1951). Baumgardner and Rodi (1989) compared tunnel measurements of the Ludlam limit with theoretical calculations and showed that the RID response tended to level off when the Ludlam limit was reached. Brown (1982) showed that the Ludlam limit would restrict the ability to infer LWC for cumulus clouds with LWC >1 g m^{-3}, but for stratiform clouds at temperatures between −5 and −10°C, the RID would normally be able to provide a reasonable estimate of LWC. Mazin et al. (2001) present a theoretical formulation applied to the RID. They showed that at temperatures between −1 and −5°C, the Ludlam limit would range from 0 to 0.17 g m^{-3} for a droplet distribution with an MVD of 15 μm. Figure 12 shows an example of how the RID signal can be highly

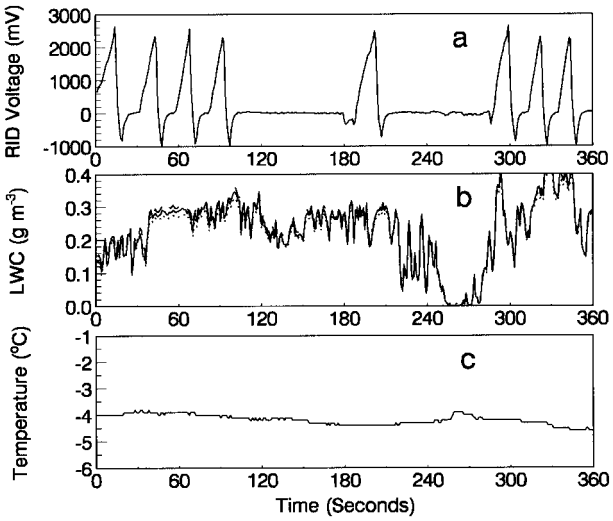

FIG. 12. Time history of (a) RID voltage, (b) LWC measured with three probes, and (c) temperature for a 360-s period from a flight on 17 Mar 1995.

variable when the Ludlam limit is reached. It shows a 360-s period during a flight on 17 March 1995. While the LWC remained relatively constant between 40 and 200 s, the RID signal remained flat between 110 and 180 s. The ambient temperature was relatively constant at −4°C, and the aircraft maintained level flight throughout this period. The response of the RID between 110 and 180 s appears to be quite inconsistent with the signal between 40 and 90 s or between 300 and 360 s, even though the temperature and LWC values were similar. Considering that ice growth near 0°C is extremely sensitive to small changes in temperature, it is believed that when the RID encounters a sustained LWC in excess of the Ludlam limit at relatively warm temperatures, the heat transfer between the freezing drops, cooling RID (warmed from the heater cycle), and dynamic heating can combine to prevent ice accumulation for an extended period of up to approximately 60 s. This conclusion is speculative and represents an area for additional research with a heat and mass transfer model similar to Mazin et al. (2001).

Because a significant portion (42%) of the in-cloud CFDE I and III data had temperatures between 0° and −5°C, the in situ data were used to assess the Ludlam limit for relatively low LWC cases. The observations could also be compared with the theoretical results of Mazin et al. (2001). Figure 13 shows the change in RID response with temperature for two LWC intervals, including 0.10–0.15 g m^{-3} and 0.25–0.30 g m^{-3}, respectively. The RID signal was converted to an LWC using the in situ k coefficient derived in section 4d. The average RID LWC–measured LWC ratio for 0.5°C temperature intervals are also shown in Fig. 13. While there is considerable scatter in the data, the falloff of the RID response with increasing temperature can clearly be observed. The temperature interval at which the falloff starts (i.e., the Ludlam limit) can be identified as the point on the temperature axis where the data falloff on the RID LWC–measured LWC = 1.0 line. These intervals are shown by the thick bars in Fig. 13. Figure 14 shows the Ludlam limit variation with LWC and temperature as well as the theoretical results of Mazin et al. (2001). The LWC for the theoretical curve was increased by 1.24 to account for the LWC enhancement effect discussed in section 4d. The curve is quite similar to the in situ measurements, although it underestimates the data by approximately 20%. This is likely caused by the surface roughness coefficient for the ice, which was assumed to be 1.0 by Mazin et al. (2001).

i. LWC threshold

Mazin et al. (2001) showed that at airspeeds of 100 m s^{-1}, the rates of sublimation and accretion would be

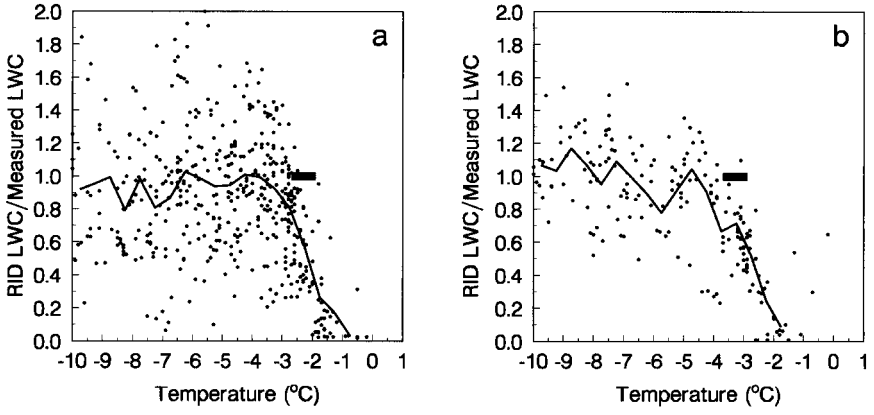

FIG. 13. Falloff of the RID response with temperature for LWC intervals of (a) 0.10 to 0.15 g m^{-3} and (b) 0.25 to 0.30 g m^{-3}. The RID LWC was computed assuming the best fit given in Fig. 6a. The thick bars represent the estimated temperature interval that the falloff occurs due to the Ludlam limit. The thin curves represent the average RID LWC–measured LWC ratio for each 0.5°C temperature interval.

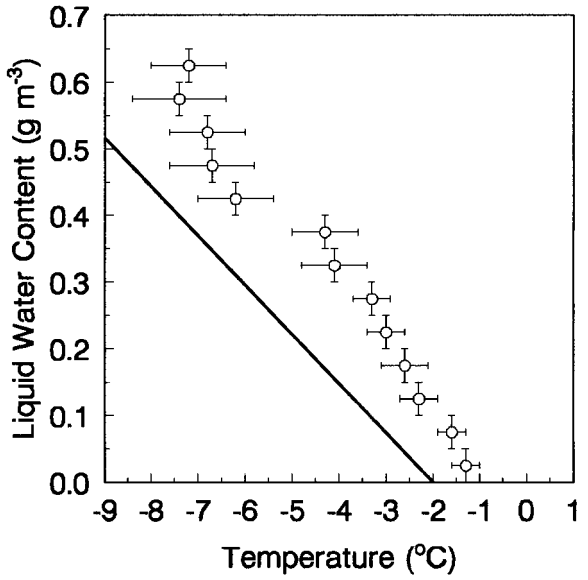

FIG. 14. Estimate of the temperature falloff at which the RID LWC–measured LWC ratio demonstrated in Fig. 13 occurs for each LWC interval. The solid curve represents the theoretical Ludlam limit as estimated by Mazin et al. (2001) for a pressure of 80 kPa and V_e of 97 m s^{-1}. The theoretical LWC values were enhanced by 24% to account for the effect of the RID mounting location on the Convair-580.

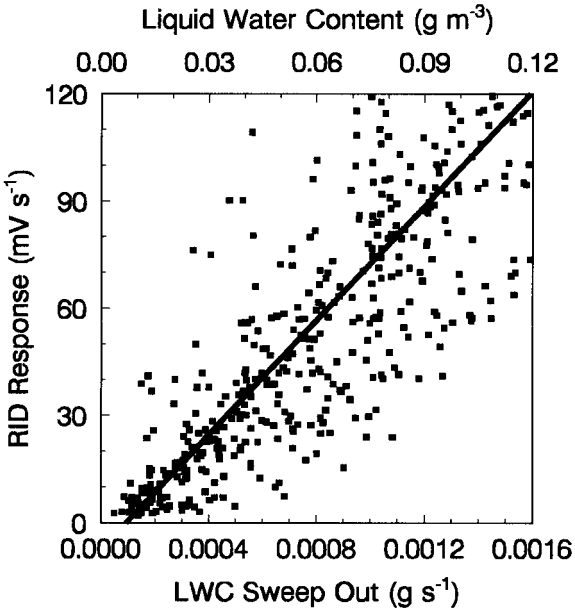

FIG. 15. Scatterplot of LWC sweep out vs RID for liquid phase cases with LWC <0.15 g m^{-3} and temperature <-5°C (485 points). The best fit has an LWC of 0.007 $\pm$ 0.010 g m^{-3} for an RID signal of 0 mV. The equivalent LWC is shown for comparison.

equal for LWC values between 0.002 and 0.006 g m^{-3}, depending on the ambient temperature, relative humidity, and pressure. For the LWC values <0.1 g m^{-3} (shown in Fig. 6a), the majority of the data fall below the best-fit curve, which is consistent with a nonzero LWC threshold. Figure 15 shows a scatterplot of RID versus an LWC sweep out for liquid phase cloud cases with LWC <0.15 g m^{-3}. The best fit has an RID signal of 0 mV at an LWC of 0.007 $\pm$ 0.010 g m^{-3}. While the LWC measurements are accurate within ± 0.02 g m^{-3}, there is not expected to be a bias toward positive or negative LWC values. Hence, it is concluded that the data shown in Fig. 15 support the predictions of Mazin et al. (2001). While theoretical formulations, such as that of Mazin et al. (2001), could be used to correct for the sublimation term when computing LWC from an RID, the $\pm 50\%$ accuracy in the LWC measurement will negate this requirement in most cases.

5. Conclusions

Using in situ observations from several research flights and the results from two series of wind tunnel experiments, the capabilities of the MSC Rosemount Icing Detector have been assessed. The observed cloud environments included a wide range of conditions, including freezing drizzle and freezing rain conditions, LWC from 0 to 0.7 g m^{-3}, temperature from 0° to -29°C, and MVD from 10 to 1000 μm. A significant limitation in this assessment is that the data are centered around a V_e of 97 m s^{-1} so that the conclusions may not be entirely applicable for aircraft that travel at significantly faster rates. In addition, the unique mounting location of the RID on the Convair-580 and the recognized requirement to calibrate each RID separately in a wind tunnel (Baumgardner and Rodi 1989) would need to be considered before the results presented here are fully applied to other Rosemount icing detectors. The following conclusions have been identified.

1) When the data are considered at 1-s resolution, 80% of the measurements in clear air are within ± 2 mV of the mean zero signal. When the data are averaged at 30 s resolution, the signal level on the MSC RID is within ± 2 mV s^{-1} or 0.002 g m^{-3} of the mean zero signal. This threshold accounts for 99.6% of the observations in clear air and 98.5% of the observations in glaciated clouds.
2) Following each de-icing cycle, the RID voltage signal is reliable and correlates linearly with LWC when it exceeds 400 mV above the clear-air voltage signal. This threshold is independent of LWC and temperature. This allows the start time for acceptable RID data following a de-icing cycle to be clearly identified when LWC measurements are being inferred from the RID signal.
3) The duration of the de-icing cycle averaged 15 $\pm$ 4 s, including the time from the start of the de-icing cycle to the point where the RID signal rose to 400 mV above the clear-air voltage signal. The duration decreased slightly with increased LWC and decreased strongly with decreasing ambient tempera-

ture. It ranged from 13 ± 4 s for temperatures <-6°C to 19 ± 3 s for temperatures between -1° and -3°C. These trends are consistent with the expected heat transfer for the RID cylinder. At temperatures colder than -18°C, the RID can require 2 or more de-icing heater cycles in order to fully clear the accumulated ice.

4) The correlation between the RID signal and LWC was linear; however, it changed from 61.6 V g^{-1} for the wind tunnel experiments to 81.0 V g^{-1} for the in situ data. Different averaging intervals between 5 and 120 s in duration did not affect the observed slopes. Considering the mounting location of the RID under the wing on the Convair-580, it is speculated that this is a region of enhanced LWC presumably caused by the compression and acceleration of the airflow under the wing. The difference in the RID–LWC slopes suggests that this enhancement could be as high as 24%.
5) For in situ data with LWC >0.1 g m^{-3}, 92% of the data fell within ±50% of the RID–LWC best fit. This scatter is related to the in-cloud variability of temperature, LWC, V_e, and MVD. Regardless, considering the simplicity of the RID, an LWC accuracy of ±50% would be extremely beneficial for assessing the accuracy of icing forecast algorithms. The observed relationship between the RID signal and LWC also applied to the observed freezing precipitation environments with MVD >100 μm.
6) The mounting location on the NRC Convair-580 aircraft appears to be free of significant shadowing effects, and there was no degradation of the RID response during ascents, descents, or turns. The presumed LWC enhancement observed on the Convair-580 suggests that the mounting location needs to be carefully selected, and RID calibrations for LWC will be highly aircraft dependent.
7) At a V_e of approximately 100 m s^{-1}, any RID response to ice particles cannot be distinguished from the mean clear-air signal. Ice crystals did not appear to erode ice accumulation or accrete to the RID surface under the range of conditions observed. Therefore, the RID can be used to estimate the LWC within ±50% in mixed phase conditions and to screen glaciated conditions. A threshold of >2 mV s^{-1} for in-cloud observations is a reasonable indicator for the presence of supercooled liquid water, while a threshold of <2 mV s^{-1} is a reasonable indicator for the absence of supercooled water.
8) The in situ data were used to infer the temperature at which the Ludlam limit was reached for LWC between 0 and 0.6 g m^{-3}. The results were within 20% of the theoretical formulations of Mazin et al. (2001). The difference between the two was probably caused by the surface roughness coefficient used by Mazin et al. (2001).
9) The in situ data suggest that the LWC threshold for the RID mounted on the Convair-580 is 0.007 ± 0.010 g m^{-3}. This was valid for measurements made with a V_e of approximately 100 m s^{-1}. The LWC threshold is consistent with the predictions of Mazin et al. (2001).

With respect to down-linking icing detector data using a system such as ACARS, it can be concluded that the data would be extremely useful if they were provided by aircraft with a V_e around 100 m s^{-1}. The low noise level, low LWC threshold, linear response of the RID to LWC for icing conditions below the Ludlam limit, ±50% LWC accuracy, and ability to infer LWC in liquid, mixed, and freezing precipitation conditions would allow useful assessments of the icing environments, which could be used for both real-time warnings and numerical icing forecast algorithm validations. Unfortunately, the majority of aircraft that are currently equipped with ACARS have V_e significantly greater than 100 m s^{-1}. At higher V_e, the LWC threshold increases, and the dynamic heating increases as V_e^2. The latter affects the Ludlam limit and reduces the range of temperatures over which the RID can detect icing. Ideally, this investigation should be repeated with an instrumented aircraft that has a substantially higher V_e in order to quantify these effects.

Acknowledgments. This work was supported by the Canadian National Search and Rescue Secretariat, Transport Canada, the National Research Council, and the Meteorological Service of Canada. The authors would like to acknowledge Dave Marcotte for assistance in determining the mounting locations of the RID on the Convair-580.

REFERENCES

Ashenden, R., and J. D. Marwitz, 1998: Characterizing the supercooled large droplet environment with corresponding turboprop aircraft response. *J. Aircraft,* **35,** 912–920.

Bain, M., and J. F. Gayet, 1982: Aircraft measurements of icing in supercooled and water droplet/ice crystal clouds. *J. Appl. Meteor.,* **21,** 631–641.

Baumgardner, D., 1983: An analysis and comparison of five water droplet measuring instruments. *J. Climate Appl. Meteor.,* **22,** 891–910.

——, and A. Rodi, 1989: Laboratory and wind tunnel evaluations of the Rosemount icing detector. *J. Atmos. Oceanic Technol.,* **6,** 971–979.

Biter, C. J., J. E. Dye, D. Huffman, and W. D. King, 1987: The drop-size response of the CSIRO liquid water probe. *J. Atmos. Oceanic Technol.,* **4,** 359–367.

Brown, E. N., 1982: Ice detector evaluation for aircraft hazard warning and undercooled water content measurements. *J. Aircraft,* **19,** 980–983.

Cober, S. G., G. A. Isaac, and J. W. Strapp, 1995: Aircraft icing measurements in east coast winter storms. *J. Appl. Meteor.,* **34,** 88–100.

——, ——, A. V. Korolev, J. W. Strapp, and D. L. Marcotte, 1999: Measurements of aircraft icing environments which include supercooled large drops. *37th Aerospace Sci. Meeting,* Reno, NV, AIAA Paper 99-0494.

——, ——, ——, and ——, 2000: Assessing the relative contribu-

tions of liquid and ice phases in winter clouds. *Proc. 13th Int. Conf. on Clouds and Precipitation,* Reno, NV, 689–692.

Cooper, W. A., W. R. Sand, M. K. Politovich, and D. L. Veal, 1984: Effects of icing on performance of a research aircraft. *J. Aircraft,* **21,** 708–715.

Drummond, A. M., and J. I. MacPherson, 1985: Aircraft flow effects on cloud drop images and concentration measured by the NAE Twin Otter. *J. Atmos. Oceanic Technol.,* **2,** 633–643.

Finstad, K. J., and E. P. Lozowski, 1988: A computational investigation of water droplet trajectories. *J. Atmos. Oceanic Technol.,* **5,** 160–170.

Fleming, R. J., 1996: The use of commercial aircraft as platforms for environmental measurements. *Bull. Amer. Meteor. Soc.,* **77,** 2229–2242.

Gardiner, B. A., and J. Hallett, 1985: Degradation of in-cloud forward scattering spectrometer probe measurements in the presence of ice particles. *J. Atmos. Oceanic Technol.,* **2,** 171–180.

Guan, H., S. G. Cober, and G. A. Isaac, 2001: Verification of supercooled cloud water forecasts with in situ aircraft measurements. *Wea. Forecasting,* **16,** 145–155.

Heymsfield, A. J., and L. M. Miloshevich, 1989: Evaluation of liquid water measuring instruments in cold clouds sampled during FIRE. *J. Atmos. Oceanic Technol.,* **6,** 378–388.

Hill, G. E., 1991: Comparison of simultaneous airborne and radiometric measurements of supercooled liquid water. *J. Appl. Meteor.,* **30,** 1043–1046.

Isaac, G. A., S. G. Cober, A. V. Korolev, J. W. Strapp, A. Tremblay, and D. L. Marcotte, 1999: Canadian Freezing Drizzle Experiment. *AIAA 37th Aerospace Sci. Meeting and Exhibit,* Reno, NV, AIAA Paper 99-0494.

Kelsch, M., and L. Wharton, 1996: Comparing PIREPs with NAWAU turbulence and icing forecasts: Issues and results. *Wea. Forecasting,* **11,** 385–390.

King, W. D., 1986: Air flow around PMS canisters. *J. Atmos. Oceanic Technol.,* **3,** 197–198.

——, D. A. Parkin, and R. J. Handsworth, 1978: A hot wire liquid water device having fully calculable response characteristics. *J. Appl. Meteor.,* **17,** 1809–1813.

——, J. E. Dye, J. W. Strapp, D. Baumgardner, and D. Huffman, 1985: Icing wind tunnel tests on the CSIRO liquid water probe. *J. Atmos. Oceanic Technol.,* **2,** 340–352.

Korolev, A. V., J. W. Strapp, and G. A. Isaac, 1998a: Evaluation of the accuracy of PMS optical array probes. *J. Atmos. Oceanic Technol.,* **15,** 708–720.

——, ——, ——, and A. N. Nevzorov, 1998b: The Nevzorov airborne hot-wire LWC–TWC probe: Principles of operation and performance characteristics. *J. Atmos. Oceanic Technol.,* **15,** 1495–1510.

Ludlam, F. H., 1951: The heat economy of a rimed cylinder. *Quart. J. Roy. Meteor. Soc.,* **77,** 663–666.

Mazin, I. P., A. V. Korolev, A. Heymsfield, G. A. Isaac, and S. G. Cober, 2001: Thermodynamics of icing cylinder for measurements of liquid water content in supercooled clouds. *J. Atmos. Oceanic Technol.,* **18,** 543–558.

Miller, D., T. Ratvasky, B. Bernstein, F. McDonough, and J. W. Strapp, 1998: NASA/FAA/NCAR supercooled large droplet icing flight research: Summary of winter 96–97 flight operations. *AIAA 36th Aerospace Sci. Meeting and Exhibit,* Reno, NV, AIAA Paper 98-0577.

Politovich, M. K., 1989: Aircraft icing caused by large supercooled droplets. *J. Appl. Meteor.,* **28,** 856–868.

Riley, R. K., T. Lindholm, M. Politovich, B. Brown, and J. W. Strapp, 1999: Prospects for the acquisition of icing data from operational aircraft. U.S. Department of Transportation Rep. DOT/FAA/AR-99/66, 13 pp.

Sand, W. R., W. A. Cooper, M. K. Politovich, and D. L. Veal, 1984: Icing conditions encountered by a research aircraft. *J. Climate Appl. Meteor.,* **23,** 1427–1440.

Schwartz, B., 1996: The quantitative use of PIREPs in developing aviation weather guidance products. *Wea. Forecasting,* **11,** 372–384.

Stewart, R. E., 1991: Canadian Atlantic Storms Program: Progress and plans of the meteorological component. *Bull. Amer. Meteor. Soc.,* **72,** 364–371.

Strapp, J. W., P. Chow, M. Maltby, A. D. Bezer, A. V. Korolev, I. Stromberg, and J. Hallett, 1999: Cloud microphysical measurements in thunderstorm outflow regions during Allied/BAE 1997 flight trials. *AIAA 37th Aerospace Sci. Meeting and Exhibit,* Reno, NV, AIAA Paper 99-0498.

——, J. Oldenburg, R. Ide, S. Bacic, and L. Lilie, 2000: Measurements of the response of hot wire LWC and TWC probes to large droplet clouds. *Proc. 13th Int. Conf. on Clouds and Precipitation,* Reno, NV, 181–184.